Rashba induced magnetoconductance oscillations in the $LaAlO_3$-$SrTiO_3$ heterostructure

A. Fête,[1] S. Gariglio,[1] A. D. Caviglia,[1,2] J.-M. Triscone,[1] and M. Gabay[3]

[1]*Département de Physique de la Matière Condensée, University of Geneva, 24 Quai Ernest-Ansermet, 1211 Genève 4, Switzerland*
[2]*Max-Planck Research Group for Structural Dynamics - Center for Free Electron Laser Science, University of Hamburg, Germany*
[3]*Laboratoire de Physique des Solides, Bat. 510, Université Paris-Sud 11, Centre d'Orsay, 91405 Orsay Cedex, France*

We report measurements of the normal state in-plane magnetoconductance in gated $LaAlO_3$-$SrTiO_3$ samples. As the orientation of the magnetic field changes within the plane of the interface, the signal displays periodic oscillations with respect to the angle between the field and the direction of the current. We show that in the underdoped to optimally doped range, a Fermi surface reconstruction takes place due to the Rashba spin-orbit term and that the oscillations are due to a magnetic field induced opening and closing of a gap at the Γ point for those Ti out-of-plane orbitals having their band minimum close to the Fermi energy of the system.

In response to a strong worldwide demand for powerful portable electronic devices, engineers have designed novel architectures for processors while shrinking their sizes and slashing down the required energy input. Current technology is still mainly silicon-based, but alternative strategies are being actively pursued which involve materials like graphene or transition metal oxides [1–3]. The latter are endowed with an incredible variety of functional properties which are extremely sensitive to structural distortions, electronic correlations and crystal chemistry. Recently a number of novel phenomena at complex oxide interfaces has been discovered [3] and among the driving forces that appear to be at play for these new observed effects are charge confinement/deconfinement in multiple valence heterostructures. Moreover these artificial structures can help us control the carrier flow by manipulation of the spin.

One promising candidate is the $LaAlO_3$-$SrTiO_3$ (LAO/STO) heterostructure. Both compounds are band insulators, yet, when a LAO film (4 or more unit cells thick) is deposited layer by layer on top of a (001) STO substrate, the heterostructure becomes metallic with an electron-like character [4, 5]. Following the growth procedure defined in Ref. 6, one finds that the conducting sheet is confined to a few nanometers on the STO side of the interface, and that superconductivity sets in below a critical temperature T_c in the 0.1 K range [7, 8]. Carrier transport was successfully modulated by applying a gate voltage V in top- [9] and back-gate geometries revealing the existence of a (zero temperature (T)) quantum critical point (QCP) for $V \equiv V_c$ separating an insulating state from a superconducting state [10] (see Figure 1(a)). At low T, in the normal state, charge transport is well described by $2D$ weak localization (WL) in a broad range of gate voltages that extends beyond V_c (underdoped regime), but it displays anomalous metallic behavior (AM) for large enough values of V (optimally doped regime). Upon increasing V, a steep rise of a Rashba-type spin-orbit contribution was evidenced beyond V_c, which appears to track the increase in T_c and the onset of AM above the dome.

In this letter we provide further experimental evidence of the role of the Rashba spin-orbit coupling on the magnetotransport properties of the LAO/STO interface. We present transport measurements for $V > V_c$, and we bring out in full view the remarkable oscillations of the magnetoconductance (MC) that take place when a magnetic field B is applied parallel to the interface and then rotated within that plane. We correlate the onset of the AM with the emergence of a spin-orbit driven Fermi surface reconstruction. In this regime, as $Ti\ d_{xz}, d_{yz}$ orbital sub-bands are being filled upon increasing V, we contend that the observed oscillations of the MC are due to the periodic opening and closing of gaps at the Γ point of $Ti\ d_{xz}$ orbital sub-bands having their band minimum very close to the Fermi energy. The amplitude of the oscillations allows one to extract a spin-orbit energy in agreement with the WL analysis.

LAO/STO interfaces were prepared by pulsed laser deposition [11]. A photolithographic process was used to define Hall bars for four points DC transport measurements performed at 1.5 K in a cryostat equipped with a rotating sample probe and a 7 T superconducting magnet. Field effect devices were created using the STO substrate as gate dielectric depositing a gold contact on the backside. The current was applied along the [100] direction and for perpendicular magnetoconductance the magnetic field was set out of plane along the [001] direction. For angular magnetoconductance, the magnetic field was applied in plane and rotated from parallel ($B \parallel$[100], ϕ=0) to perpendicular ($B \parallel$[010], ϕ=$\pi/2$) to the current (see Figure S1 in supplementary material).

When the applied magnetic field B is perpendicular to the interface, the B dependence of the measured MC is quantitatively captured using a WL expression for non interacting fermions [1] in a broad range of gate voltages

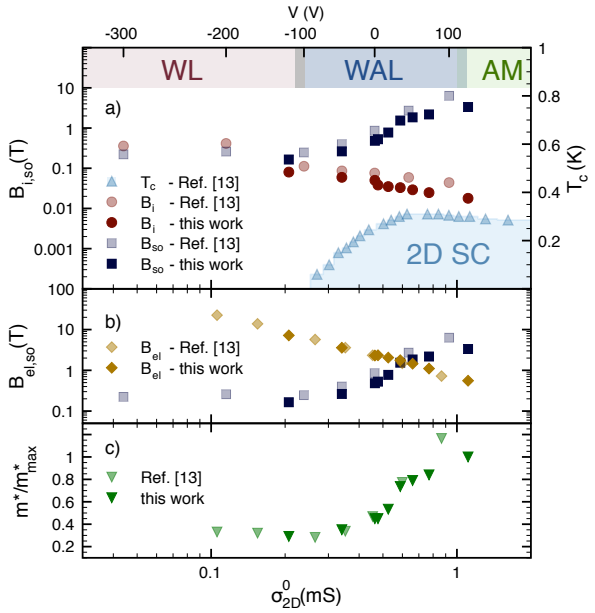

FIG. 1: (color online) (a) Evolution of the inelastic (B_i) and spin-orbit (B_{so}) fields as a function of σ^0_{2D} (the sheet conductance at B=0) for the sample of this work and a reference sample (data from Ref. 13) in the diffusive regime. The top voltage scale indicates the corresponding applied voltages for the reference sample. The superconducting phase (2D SC, blue region) and the transition temperature T_c (triangles) are also shown. (b) Evolution of the elastic (B_{el}) and spin-orbit fields with σ^0_{2D} highlighting the crossing at $\sigma^0_{2D} \sim 0.6$ mS. Data points extend slightly beyond the diffusive regime. (c) variation of the transport effective mass m^* with σ^0_{2D}. Here ${m^*}_{max} \sim 2.2m_e$. WL, WAL, AM shaded regions denote the weak localization, weak antilocalization and anomalous metal regimes respectively.

extending beyond V_c. The accuracy of the fit allows us to estimate the values of the inelastic field, B_i and of the spin-orbit field B_{so} as a function of the gate voltage.

Figure 1 (a) displays the evolution of these two quantities versus σ^0_{2D}, the sheet conductance (well suited for comparing data from different samples).

Previous studies [13, 14] have shown that the origin of the spin-orbit part stems from a Rashba interface term. Accordingly, we can determine the effective Drude mass m^* using the D'yakonov-Perel' relation between the spin-orbit (τ_{so}) and elastic (τ) scattering times $\frac{2\pi}{\tau_{so}} = {\Omega_{so}}^2\tau$, where $\Delta_{so} \equiv \hbar\Omega_{so} = 2\lambda E k_F$ is the Rashba energy (λ is the material specific Rashba spin-orbit coefficient, E is the interfacial electric field along z, the direction normal to the interface, k_F is the Fermi momentum)[4]

$$m^* = \frac{h^2}{4\pi\lambda E}\sqrt{\frac{B_{so}}{\Phi_0}} \qquad (1)$$

($\Phi_0 = \frac{h}{2e}$) and hence τ (or B_{el} the elastic magnetic field) in the WL regime (see supplementary material).

When Eq.(3) holds, i.e. in the range of V such that spin-orbit terms contribute to diffusive processes, we consider that λ has little V dependence. By contrast, changing the gate voltage modifies the sheet carrier density n_S and causes a variation of E. The change in E can be determined from an electrostatic model of the confined electron gas [16], taking into account the electric field dependence of the STO dielectric constant (see Ref. 17).

Using these prescriptions, we present the variations of B_{el}, B_{so} and m^* with σ^0_{2D} (or V) in Figures 1 (b) and (c). To highlight the trends, we include data points slightly beyond the diffusive regime (see below). We note that m^* is ~ 3.5 lighter in the underdoped regime than in the optimally doped regime, which is consistent with the picture of an interface charge transport evolving from being d_{xy}-dominated ($m^* \sim 0.64m_e$ [6], m_e is the bare electron mass) to being d_{xz}/d_{yz}-dominated ($m^* \sim 2.2m_e$), upon increasing V beyond $\sigma^0_{2D} \sim 0.5$ mS [13, 14, 19–23]. The concomittant rise in τ (Figure S2 supplementary material) fits with this picture, since it signals that additional conduction channels start contributing. As reported in Refs. ([13, 14]), τ_{so} decreases steeply across V_c, to the extent that $\tau_{so} \sim \tau$ for $\sigma^0_{2D} \sim 0.6$ mS (Figure 1 (b)). When this occurs spin-orbit processes cease to be diffusive. The spin-orbit time is no longer given by the D'yakonov-Perel' expression and the Rashba term becomes a *bona fide* new energy scale in the problem, on equal footing with the kinetic part. Band structure needs to be recalculated in the presence of the (Fermi surface reconstructing) Rashba hamiltonian. The evolution towards this AM regime is suggestive of a scenario of spin-orbit protected transport (against disorder) in the 2D conducting sheet.

Ab-initio density functional theory (DFT) band structure calculations have been carried out for the LAO/STO system [5, 23–25]. These studies reveal that the conduction band consists of a manifold of t_{2g} states originating from a decomposition of the t_{2g} triplet into sub-bands, in response to the interfacial confining electric field [6, 17, 27]. The energy minima of these sub-bands are located at the Γ point; the lower the value of the energy at the minimum the closer to the interface along z the wavefunction is. According to Ref. ([5]), for values of $n_S \sim 10^{14}$ cm^{-2} the states which lie closest to the interface, i.e. which do not extend beyond the first 3 unit cells from the STO boundary, on the STO side, have d_{xy} symmetry and account for a large part of the carrier concentration. d_{xz}, d_{yz} sub-bands spread out deeper into the (STO) bulk, and, as they are being filled, they contribute to n_S on the order of 10^{13} cm^{-2}. These out of plane orbitals lie close the Fermi surface and we argue below that they control charge transport in the AM regime.

To showcase the significant role played by the d_{xz}, d_{yz} states, we measure the angular MC of the 2DEG when a magnetic field is applied in plane and rotated from parallel to perpendicular to the current. In this geometry the magnetotransport is not affected by orbital contribu-

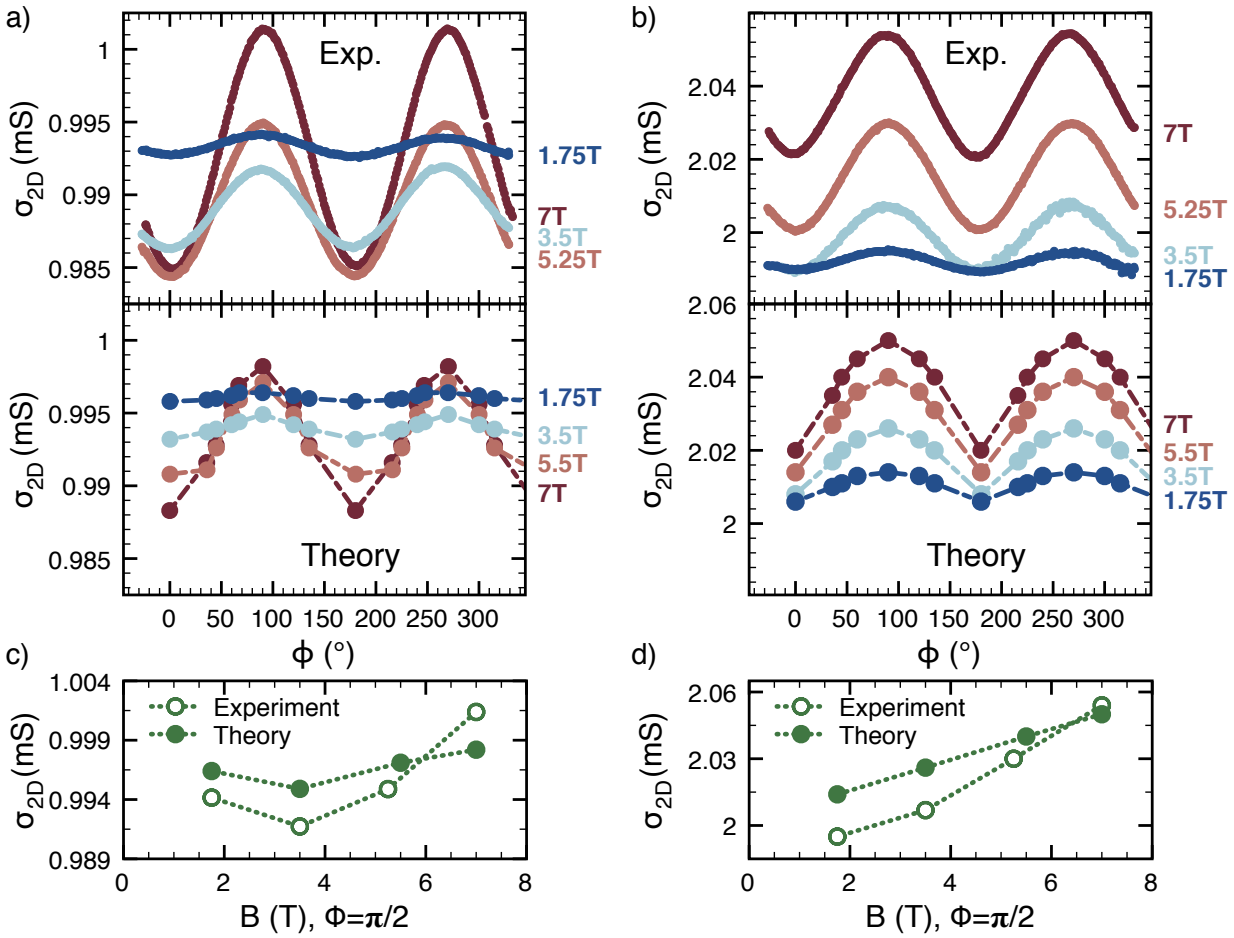

FIG. 2: (color online) (a) and (b) Experimental and theoretical plots of the conductance $\sigma_{2D}(B,\phi)$ versus ϕ, the angle between the in-plane magnetic field B and the current for various values of B. (a) corresponds to $\sigma^0_{2D} = 1$ mS and (b) to $\sigma^0_{2D} = 2$ mS. (c) and (d) are experimental and theoretical dependence of the conductance on the in-plane magnetic field for $\phi{=}\pi/2$.

tions. Figure 2 shows the variation of the conductance with the angle ϕ for four values of the magnetic field when σ^0_{2D} is 1 mS (a)) and σ^0_{2D} is 2 mS (b)). Maxima of the conductance are seen for both dopings when the external magnetic field is applied perpendicularly to the current. However the maximum of the oscillation $\sigma_{2D}(B,\phi=\pi/2)$ evolves in a non monotonic way for the first doping which is not case for the higher conductance state. Note that oscillations of the MC in the parallel field geometry have been reported by Ben Shalom et al ([28]). For the range of sheet conductances and the field intensity that they considered (typically higher than ours) they found a positive MC for $\phi = 0$, and suggested that a magnetic order forms at the interface.

For the doping range considered here, we may understand the behavior of the parallel MC as the field is rotated within the **xy** plane if we note that carriers in the d_{xz} or d_{yz} sub-bands have one light and one heavy mass ($m_h \sim 20m_e$) [6, 19]. Thus, qualitatively, the d_{xz} and d_{yz} orbitals are 1D-like and, since current flows along **x**, we focus on the former type which gives a higher contribution to transport. In the presence of the Rashba term, the spin-split bands exhibit an energy gap at the Γ point when B is along **x** ($\phi = 0$) and a Zeeman-like offset when B is along **y** ($\phi = \frac{\pi}{2}$) (Figure S3 supplementary material). The impact of this effect on transport depends on the position of E_F relative to E_Γ, the energy of the electronic states at the Γ point when $B = 0$, since the density of states (DOS) at the Fermi energy, $g(E_F)$, enters the expression of σ_{2D}. The conductivity will thus show a dip for $\phi = 0$, provided $E_F \sim E_\Gamma$. If E_F is not close to E_Γ, $g(E_F)$ is almost unchanged as compared to its $B = 0$ value. As mentioned in the previous section, in the underdoped to optimally doped range, E_Γ of most of the sub-bands with a d_{xy} character is well below E_F. Yet, the E_Γ of d_{xz} symmetry bands are close to E_F. So the Rashba induced modulation of $g(E_F)$ is controlled by the change in the d_{xz} carrier DOS. Insofar as one may reasonably assume that τ does not depend on B in the 2D case, one expects a periodic variation of the MC with

ϕ, displaying crests for B along **y** and troughs for B along **x**.

In the framework of this 1D picture and with the additional simplifying assumption that the variation of σ_{2D} with ϕ is entirely due to the d_{xz} sub-band closest to E_F, we find $(\sigma_{2D}(B,\phi=\pi/2)-\sigma_{2D}(B,\phi=0))/\sigma_{2D}(B,\phi=0) = 1/8(\Delta_{so}/E_F)^2$ when the Zeeman energy is larger than the condensation energy of the Rashba state (Δ_{so}) (see also [29]). Beyond the qualitative 1D model, we have modelled the evolution of the band structure for the t_{2g} orbitals in the applied B. We use a tight binding model featuring kinetic and Rashba terms and we take into account the finite value of m_h and the anisotropy of λ in the **xy** plane for the d_{xz}, d_{yz} orbitals. The mobility, λ and the gyromagnetic factor g all depend on V, but we consider that they do not change appreciably with ϕ nor with the magnitude of B in our experiments. For a given V, the variation of δn – i.e. the change in the d_{xz}, d_{yz} carrier concentrations – with ϕ and B depends on the values of the spin-orbit and of the Zeeman energies. The conductance $\sigma_{2D}(B,\phi)$ is then proportional to δn. Experimental data and plots obtained from the model are shown in Figures 2 (c) and (d). We note that while $\sigma_{2D}(B,\phi)$ increases monotonically with B at fixed ϕ for $\sigma^0_{2D} = 2$ mS, such is not the case for $\sigma^0_{2D} = 1$ mS, a feature which is correctly captured by our model. Figure 3 displays the evolution of $\Delta\sigma_{2D} = \sigma_{2D}(B,\phi=\pi/2) - \sigma_{2D}(B,\phi=0)$ versus B according to our model and the experimental results. We find good agreement using $\Delta_{SO} = 7(2.5)$ meV for $\sigma^0_{2D} = 2(1)$ mS respectively. These values fall within the range of previous experimental estimates [13, 14].

Figure 4 shows the evolution of the experimental oscillation amplitude $\Delta\sigma_{2D}$ as a function of σ^0_{2D} for different magnetic fields. As can be seen, $\Delta\sigma_{2D}$ tends to zero for a sheet conductance in the $0.1-0.3$ mS range. These sheet conductance values – which lie in the diffusive regime – are close to the QCP, suggesting a potentially important role played by the d_{xz}, d_{yz} orbitals in establishing superconductivity.

In summary, our findings underscore the evolution that takes place in the $LaAlO_3$-$SrTiO_3$ heterostructure, as one tunes the gate voltage in the range where superconductivity is observed at low temperature. For low V, conduction is diffusive and is dominated by the d_{xy} orbitals, as the impact of disorder is expected to be more severe for the 1D-like d_{xz}, d_{yz} states. For larger values of V, the nature of transport changes and the out of plane d_{xz}, d_{yz} orbitals start contributing to the zero field conductivity, as evidenced by the evolution of m^*, B_{el}, B_{so} and by the oscillations of the in-plane magnetoconductance. For these orbitals, the effect of the strong spin-orbit interaction has to be taken into account at the band structure level for the calculation of their contribution to the transport.

We would like to thank M. Lopes and S. C. Müller for their technical assistance. This work was supported by the Swiss National Science Foundation through the National Center of Competence in Research, Materials with Novel Electronic Properties, MaNEP and division II, by the Institut Universitaire de France (MG), and the European Union through the project OxIDes.

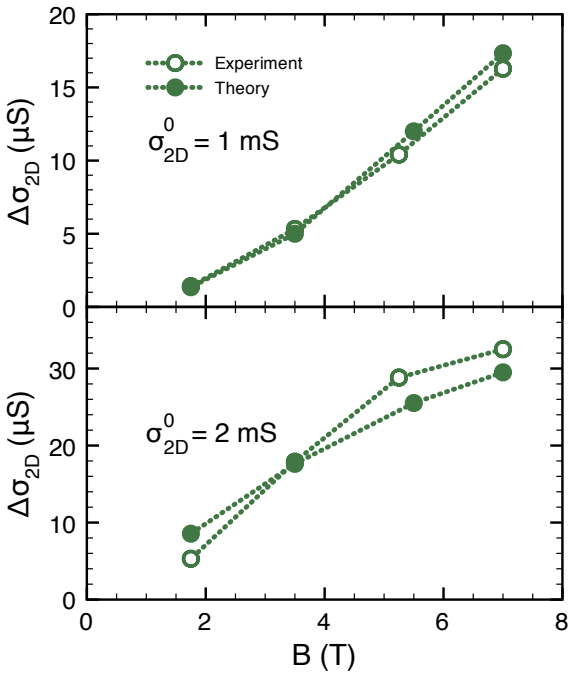

FIG. 3: (color online) Experimental and model determined plots of $\Delta\sigma_{2D}$ versus B for $\sigma^0_{2D} = 1$ mS and $\sigma^0_{2D} = 2$ mS.

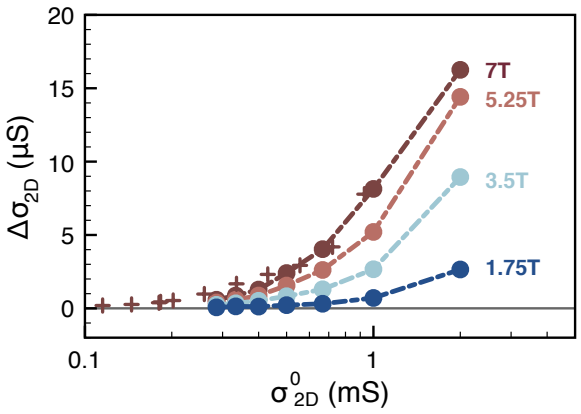

FIG. 4: (color online) Evolution of the amplitude of the experimental oscillations $\Delta\sigma_{2D}$ ($\Delta\sigma_{2D} = \sigma_{2D}(B,\phi=\frac{\pi}{2}) - \sigma_{2D}(B,\phi=0)$) as a function of σ^0_{2D} . "Plus" symbols pertain to measurements performed on an additional sample at 7 T.

[1] Ph. Avouris, Nano Lett. **10**, 4285 (2010).

[2] F. Xia, D. B. Farmer, Y.-M. Lin, Ph. Avouris, Nano Lett. **10**, 715 (2010).
[3] P. Zubko, S. Gariglio, M. Gabay, P. Ghosez, J.-M. Triscone, Annu. Rev. Condens. Matter Phys. **2**, 141 (2011).
[4] A. Ohtomo, H. Y. Hwang, Nature **427**, 423–426 (2004).
[5] S. Thiel, G. Hammerl, A. Schmehl, C. Schneider, J. Mannhart, Science **313**, 1942 (2006).
[6] C. Cancellieri, N. Reyren, S. Gariglio, A. D. Caviglia, A. Fête, J.-M. Triscone, EPL **91**, 17004 (2010).
[7] M. Basletic *et al.*, Nat. Mat. **7**, 621-625 (2008).
[8] N. Reyren *et al.*, Science **317**, 1196-1199 (2007).
[9] L. Li, C. Richter, S. Paetel, T. Kopp, J. Mannhart, R.C. Ashoori, Science **232**, 825 (2011).
[10] A. D. Caviglia *et al.*, Nature **456**, 624-627 (2008).
[11] See supplementary informations for thin films growth and characterization.
[12] S. Maekawa, H. Fukuyama, J. Phys. Soc. Jpn. **50**, 2516 (1981).
[13] A. D. Caviglia, M. Gabay, S. Gariglio, N. Reyren, C. Cancellieri, J.-M. Triscone, Phys. Rev. Lett. **104**, 126803 (2010).
[14] M. Ben Shalom, M. Sachs, D. Rakhmilevitch, A. Palevski, Y. Dagan, Phys. Rev. Lett. **104**, 126802 (2010).
[15] R. Winkler, *Spin-orbit Coupling Effects in Two-Dimensional Electron and Hole Systems*, Springer (2003).
[16] At the boundary between the WL and AM regimes, we assign to E the value reported in Ref(6), as we surmize that the field E on the STO side of the interface is caused by all the charge carriers whether they are mobile or not.
[17] K. Ueno *et al.*, Nat. Mat. **7**, 855-858 (2008).
[18] A. F. Santander-Syro *et al.*, Nature **469**, 189 (2011).
[19] S. S. A. Seo *et al.*, Appl. Phys. Lett. **95**, 082107 (2009).
[20] M. Ben Shalom, A. Ron, A. Palevski, Y. Dagan, Phys. Rev. Lett. **105**, 206401 (2010).
[21] A. D. Caviglia *et al.*, Phys. Rev. Lett. **105**, 236802 (2010).
[22] O. Copie *et al.*, Phys. Rev. Lett. **102**, 216804 (2009).
[23] R. Pentcheva, W. E. Pickett, Phys. Rev. Lett. **102**, 107602 (2009).
[24] Z. S. Popović, S. Satpathy,R. M. Martin, Phys. Rev. Lett. **101**, 256801 (2008).
[25] W.-J. Son, E. Cho, B. Lee, J. Lee, S. Han, Phys. Rev. B **79**, 245411 (2009).
[26] P. Delugas, A. Filippetti, V. Fiorentini, D. I. Bilc, D. Fontaine, P. Ghosez, Phys. Rev. Lett. **106**, 166807 (2011).
[27] W. Meevasana *et al.*, Nat. Mat. **10**, 114 (2011).
[28] M. Ben Shalom, C.W. Tai, Y. Lereah, M. Sachs, E. Levy, D. Rakhmilevitch, A. Palevski, Y. Dagan, Phys. Rev. B **80**, 140403(R) (2009).
[29] R. Raimondi, M. Leadbeater, P. Schwab, E. Caroti, C. Castellani, Phys. Rev. B **64**, 235110 (2001).

Supplementary Information

SAMPLE PREPARATION AND EXPERIMENTAL GEOMETRY

A $LaAlO_3$ (LAO) layer thicker than 4 unit cells was grown on a (001) TiO_2-terminated $SrTiO_3$ (STO) substrate heated at 800°C in an oxygen pressure of 10^{-4} mbar. The KrF excimer laser fluency was set to 0.6 J/cm^2 with a repetition rate of 1 Hz. After deposition, the oxygen pressure was raised to 0.2 bar and the sample was kept at a temperature of about 530°C during 1 hour before cooling to room temperature. The layer thickness was estimated *in situ* from intensity oscillations of the reflection high energy electron diffraction (RHEED) spots.

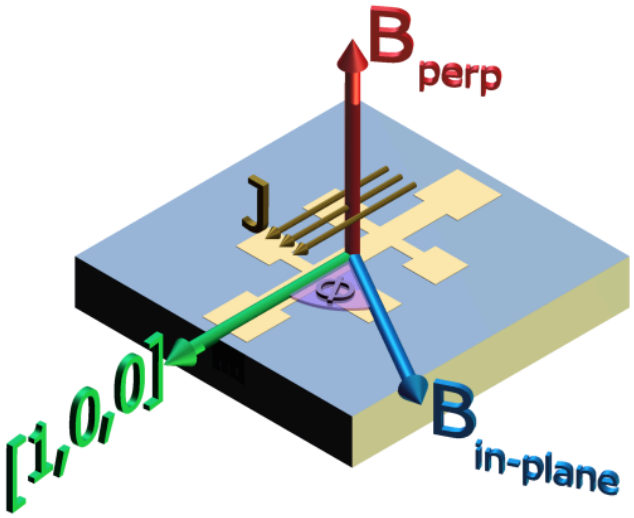

FIG. 1: Shematic view of a field effect device. ϕ is the angle between the current (J) and the in-plane magnetic field $B_{in-plane}$.

WEAK LOCALIZATION ANALYSIS

In the diffusive regime, the perpendicular magnetoconducance (MC) is quantitatively captured using weak localization corrections. We have estimated the spin-orbit field B_{so} and the inelastic field B_i as a function of the gate voltage using the Maekawa-Fukuyama expression for the magnetoconductance [1]. In order to obtain both the effective mass m^* and the bare (Drude) elastic transport time τ, we need to determine the bare conductance (σ_D^0) for various V. To that end, we use the experimentally measured $B = 0$ sheet conductance (σ_{2D}^0) and substract the zero field WL correction to the conductance, given by

$$\Delta\sigma_{WL}^0 = \frac{e^2}{\pi h}\left(Log[(1+\frac{B_{so}}{B_i})(1+\frac{2B_{so}}{B_i})^{\frac{1}{2}}] - Log[\frac{B_{el}}{B_i}]\right) \quad (2)$$

Effective mass

In order to determine m^*, we consider the D'yakonov-Perel' relation [2] between τ_{so} and τ, namely $\frac{2\pi}{\tau_{so}} = \Omega_{so}^2\tau$ where $\Delta_{so} \equiv \hbar\Omega_{so} = 2\lambda E k_F$ is the Rashba energy (E is the interfacial electric field, k_F is the Fermi momentum).

In the diffusive regime, the spin-orbit field is defined as $B_{so} = \frac{\Phi_0}{4\pi D\tau_{so}}$, where $\Phi_0 = \frac{h}{2e}$ and $D = \frac{1}{2}{v_F}^2\tau$ is the Drude (bare) diffusion constant. Using the D'yakonov-Perel' relation, it follows that $D\tau_{so} = \frac{1}{2}{v_F}^2\frac{2\pi}{\Omega_{so}^2}$. Taking into account

the fact that $m^* v_F = \hbar k_F$ and that $\Omega_{so} = \frac{2\lambda E k_F}{\hbar}$ we obtain

$$\frac{\Phi_0}{B_{so}} = 4\pi D\tau_{so} = \frac{h^4}{4\pi^2}\frac{1}{(\lambda E m^*)^2}$$

Hence

$$m^* = \frac{h^2}{4\pi\lambda E}\sqrt{\frac{B_{so}}{\Phi_0}} \tag{3}$$

Elastic scattering time

The elastic field in Eq.(2) is given by $B_{el} = \frac{\Phi_0}{4\pi D\tau}$. Using $D = \frac{1}{2}{v_F}^2\tau$, $m^* v_F = \hbar k_F$, and $k_F^2 = 2\pi n$ allows us to rewrite B_{el} in terms of the Drude mobility $\mu_D = \frac{e\tau}{m^*}$ and of the mobile sheet carrier density n. Because $\Delta\sigma^0_{WL}$ is a correction to the conductivity and because B_{el} enters Eq.(2) through a Log term, we may replace μ_D by the renormalized μ – obtained from measuring the sheet conductivity – in the expression of B_{el} when we compute $\Delta\sigma^0_{WL}$. We then subtract $\Delta\sigma^0_{WL}$ from the measured sheet conductance σ^0_{2D} to get the Drude conductivity $\sigma^0_D = ne\mu_D$. Besides, magnetotransport allows us to extract the sheet carrier density and the effective mass (Eq.(3)); from these three quantities we determine the elastic scattering time τ and its variation with σ^0_{2D} is shown in Figure 2. We note the steep rise in τ which mirrors the sharp increase in m^* beyond $\sigma^0_{2D} \sim 0.5$ mS. Such upturn may be understood if we recall that while d_{xy} orbitals appear to dominate transport for lower values of σ^0_{2D}, $d_{xz,yz}$ states contribute significantly for larger σ^0_{2D}.The steep rise suggests that the mobility of the $d_{xz,yz}$ orbitals is sizably larger than that of the d_{xy} orbitals.

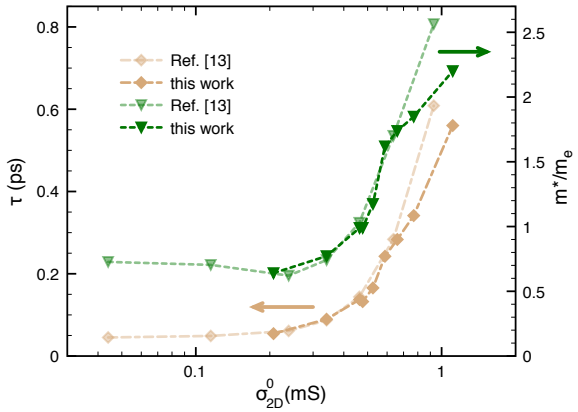

FIG. 2: Dependence of the elastic scattering time (left scale) and of the effective mass (right scale) on the sheet conductance σ^0_{2D}.

BAND STRUCTURE MODEL FOR IN-PLANE FIELD MAGNETOCONDUCTANCE

Beyond a characteristic voltage $V > V_c$, τ_{so} can become less than τ – the transport elastic time – implying that the spin-orbit term is no longer diffusive but that it changes the eigenenergies of the states. Figure 3 displays the band structure for the d_{xz} orbitals split by the Rashba coupling.

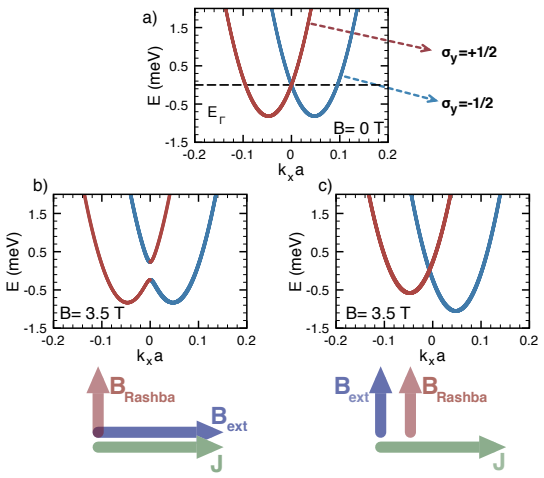

FIG. 3: Shematic view of the band structure according to our model. a) We show a d_{xz} sub-band split by a spin-orbit coupling of 5 10^{-12} eV m. The effective mass used in the calculation is $m^*_{x,xz}$=0.64 m_e. E_Γ defines the crossing point of the spin-split bands. b) Applying a magnetic field parallel to the current direction ([100] direction, $\phi = 0$) opens a gap at the gamma point: when the Fermi level is at E_Γ, the change in carrier density leads to a decrease of conductance. c) When the magnetic field is in plane and perpendicular to the current ([010] direction, $\phi = \pi/2$), a Zeeman effect is observed on the band structure.

MODELLING PARALLEL-FIELD MAGNETOCONDUCTANCE OSCILLATIONS

In order to describe the evolution of the 2DEG conduction bands as the orientation of the parallel field B changes in the plane of the interface, we use a tight-binding representation of the t_{2g} triplet states. In momentum space, the Hamiltonian has diagonal entries $\mathbf{H}_k$ consisting of 2×2 spin blocks; $\mathbf{H}_k$ contains a kinetic part

$$(2t_x(1-\cos(k_x d)) + 2t_y(1-\cos(k_y d)))\,\mathbb{1}_2 \tag{4}$$

a Rashba piece

$$\frac{\alpha_{yR}}{d}\sin(k_y d)\,\sigma_x - \frac{\alpha_{xR}}{d}\sin(k_x d)\,\sigma_y \tag{5}$$

and a Zeeman term

$$-\frac{g\mu_B}{2}B\cos\phi\,\sigma_x - \frac{g\mu_B}{2}B\sin\phi\,\sigma_y \tag{6}$$

$\mathbb{1}_2$ is the unit matrix in spin space and σ_x, σ_y, σ_z are the Pauli matrices. The angle between the in-plane magnetic field B and the x (current) direction is ϕ. d (~ 3.91Å) is the lattice spacing.

d_{xy} orbitals are invariant under a $x \leftrightarrow y$ symmetry, so that $t_x = t_y$ and $\alpha_{xR} = \alpha_{yR} = \alpha_R$. By contrast, d_{xz} and d_{yz} states are anisotropic and, from the small k limit, t_y/t_x (t_x/t_y) is equal to the ratio of the light mass m_l over the heavy mass m_h for the d_{xz} (d_{yz}) orbitals respectively. Similarly, the coefficients of the Rashba contributions are anisotropic and, following the discussion presented in Ref. [3], we account for this by setting $\alpha_{yR}/\alpha_{xR} = m_l/m_h$ ($\alpha_{xR}/\alpha_{yR} = m_l/m_h$) for the d_{xz} (d_{yz}) orbitals respectively.

$$E_\pm = 2t_x(1-\cos(k_x d)) + 2t_y(1-\cos(k_y d)) \pm \sqrt{(\frac{\alpha_{xR}}{d}\sin(k_x d) + \frac{g\mu_B}{2}B\sin\phi)^2 + (\frac{\alpha_{yR}}{d}\sin(k_y d) - \frac{g\mu_B}{2}B\cos\phi)^2} \tag{7}$$

To the above energy we must add the energy term describing the confinement in the direction perpendicular to the interface. It produces an *a priori* different value of the energy E_Γ at the Γ point for each of the d states [6]. With these energies, we may determine the occupations of the orbitals for a given value of E_F. When current flows in the x direction, we focus on the d_{xz} orbital whose E_Γ is close to E_F. If the elastic transport time does not change appreciably upon varying B and ϕ, we claim that the angular dependence of the magnetoconductance stems from the modulation of the DOS as B rotates within the plane of the interface. So we write $\sigma_{2D}(B,\phi) = \sigma^{(1)}(n) + C(n)\delta n$.

$\sigma^{(1)}(n)$ and $C(n)$ depend on the mobile carrier concentration n (on the gate voltage) but not on B or ϕ. The carrier density in the d_{xz} band whose E_Γ is close to E_F, δn ($<< n$), changes with the gate voltage, B and ϕ.

$\sigma^{(1)}(n)$ is the contribution to the conductance of those d states whose E_Γ is not close to E_F. As explained in the text, we expect negligible B and ϕ dependence in that case.

For a given σ^0_{2D} we choose one value of the field (7T for $\sigma^0_{2D} = 2$mS, 5.5T for $\sigma^0_{2D} = 1$mS) and we determine $\sigma^{(1)}(n)$, $C(n)$, α_R and g so as to best fit the experimental variation of $\sigma_{2D}(B,\phi)$ with ϕ. We subsequently use these same values when we change B and compute the new $\sigma_{2D}(B,\phi)$. A comparison between the theoretical and the experimental curves is shown in Figures 2 and 3.

[1] S. Maekawa, H. Fukuyama, J. Phys. Soc. Jpn. **50**, 2516 (1981).
[2] M. I. D'yakonov, V. I. Perel', Sov. Phys. Solid State **13**, 3023 (1972).
[3] E. Simon, A. Szilva, B. Ujfalussy, B. Lazarovits,G. Zarand, L. Szunyogh, Phys. Rev. B **81**, 235438 (2010).
[4] R. Winkler, *Spin-orbit Coupling Effects in Two-Dimensional Electron and Hole Systems*, Springer (2003).
[5] P. Delugas, A. Filippetti, V. Fiorentini, D. I. Bilc, D. Fontaine, P. Ghosez, Phys. Rev. Lett. **106**, 166807 (2011).
[6] A. F. Santander-Syro *et al.*, Nature **469**, 189 (2011).